

Seasonality in Surface Quasigeostrophic Turbulence with Variable Stratification

HOUSSAM YASSIN,^a STEPHEN M. GRIFFIES,^{a,b}

^a *Program in Atmospheric and Oceanic Sciences, Princeton University, Princeton, NJ, USA*

^b *NOAA/Geophysical Fluid Dynamics Laboratory, Princeton, NJ, USA*

ABSTRACT: Traditional surface quasigeostrophic theory assumes a vertically uniform stratification. As a consequence, the theory is only valid at horizontal scales smaller than 10 km (in the mid-latitude open ocean). At larger scales, the vertical structure of the ocean's stratification becomes important. We present a generalization of surface quasigeostrophic theory that accounts for the ocean's vertical stratification. We find that the seasonality of upper ocean stratification (in particular, the seasonality in mixed-layer depth) implies a seasonality in surface quasigeostrophic turbulence. Deep wintertime mixed-layers lead to a surface quasigeostrophic turbulence with strong buoyancy gradients, vortices spanning a wide range of scales, and with large-scale strain evident. In contrast, shallow summertime mixed-layers lead to a surface quasigeostrophic turbulence that is spatially local, lacks large-scale strain, and appears diffuse in space. The variable stratification theory also predicts a seasonal kinetic energy spectrum. If the submesoscales (1-100 km) are in the forward cascade of buoyancy variance, the theory predicts a wintertime spectrum proportional to $k^{-7/3}$. In contrast, the lack of scale invariance across the submesoscales in summer causes the cascade theory to fail. However, simulations generally suggest a kinetic energy spectrum that is flatter in summer than in winter. This seasonality is opposite to that found in the ocean at the submesoscales. We conclude by suggesting that submesoscale interior quasigeostrophic turbulence must be seasonal as well because it also depends on the vertical structure of the ocean stratification.

1. Introduction

a. Three limitations of traditional surface quasigeostrophy

Surface buoyancy anomalies induce geostrophic motion. This observation led several authors (LaCasce and Mahadevan 2006; Lapeyre and Klein 2006) to suggest that upper ocean submesoscale (1-100 km) dynamics can be described by surface quasigeostrophic theory (Blumen 1978; Held et al. 1995). However, three discrepancies have since been revealed.

The first discrepancy is that surface quasigeostrophic theory cannot account for the seasonal cycle in submesoscale turbulence. The distribution of kinetic energy across the submesoscales is correlated with mixed-layer depth (Mensa et al. 2013; Sasaki et al. 2014; Callies et al. 2015; Thompson et al. 2016; Su et al. 2018). Shallow summertime mixed-layers coincide with a k^{-3} kinetic energy spectrum (Wang et al. 2010; Callies and Ferrari 2013; Callies et al. 2015; Rocha et al. 2016) whereas deep wintertime mixed-layers coincide with a shallow k^{-2} kinetic energy spectrum (Shcherbina et al. 2013; Callies et al. 2015). Moreover, unlike in summer, the submesoscales in winter are replete with small-scale fronts and vortices. This seasonality remains unexplained in surface quasigeostrophic theory.

The second discrepancy is that surface quasigeostrophic theory predicts a kinetic energy spectrum that is too flat. If the submesoscales are assumed to be in the forward cascade inertial range of buoyancy variance, then the theory

predicts a $k^{-5/3}$ kinetic energy spectrum which is flatter than both the summertime and wintertime spectra.

The third discrepancy is that the theory cannot account for the observed vertical structure of submesoscale turbulence. Submesoscale turbulence extends, and remains uniform, throughout the whole mixed-layer; it is only below the mixed-layer that submesoscale turbulence begins to decay (Callies and Ferrari 2013; Sasaki et al. 2014; Callies et al. 2015). In contrast, in surface quasigeostrophic theory there is a rapid decay throughout the mixed-layer beginning from the ocean's surface.

However, the surface quasigeostrophic theory presented in Blumen (1978) and Held et al. (1995) assumes a vertically uniform stratification. This assumption is not valid in the ocean. Our aim in this article is to describe a surface quasigeostrophic theory that takes variable stratification into account. We then address whether this generalization can account for the above three discrepancies.

b. An example

Before we describe the theory, we first provide an example of how surface quasigeostrophic dynamics depend on ocean stratification.

Figure 1 shows two simulations forced at large scales (≈ 100 km). Both simulations have no interior potential vorticity and the dynamics are due entirely to surface buoyancy anomalies. Moreover, the two simulations differ only in stratification. One simulation has a January mean stratification at a mid-latitude location in the North Atlantic whereas the other has a July mean stratification at the same location.

Corresponding author: Houssam Yassin, hyassin@princeton.edu

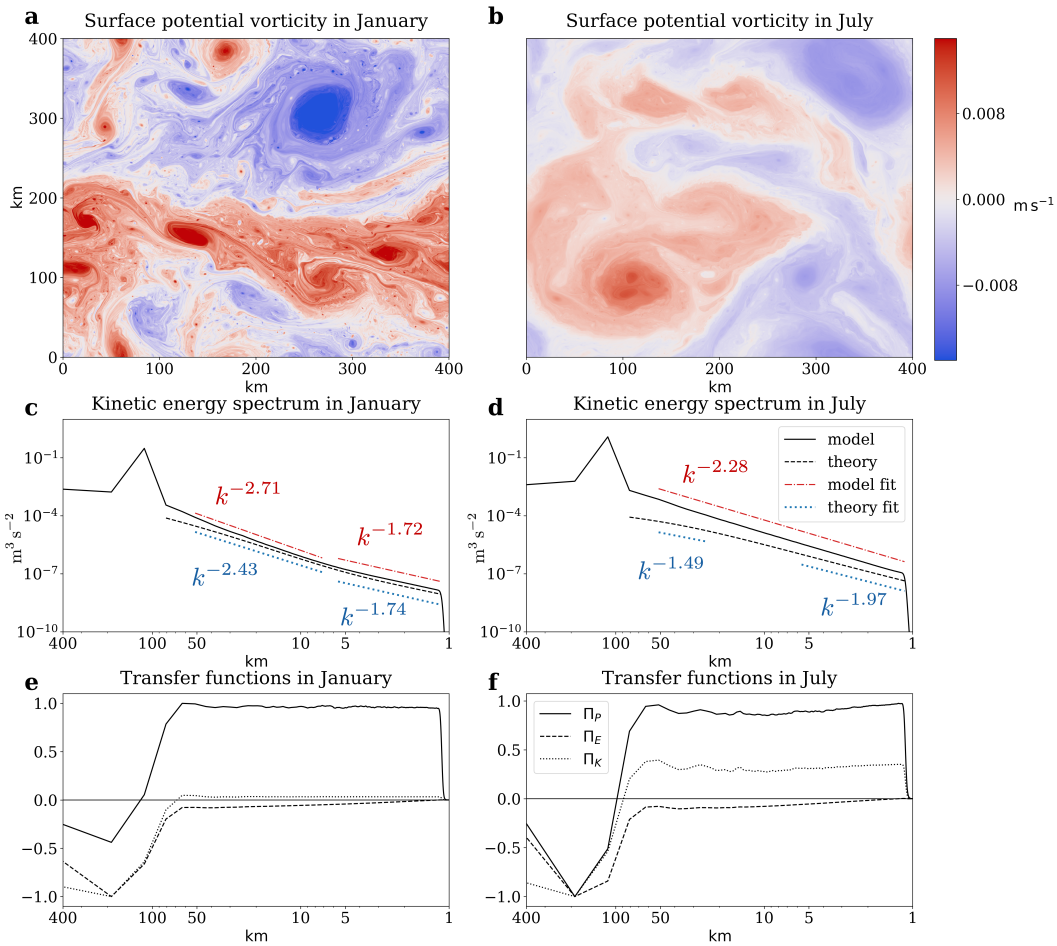


FIG. 1. Results of two pseudo-spectral surface quasigeostrophic simulations, both forced at approximately 100 km, that differ only in stratification. Both simulations have 1024^2 horizontal grid points. See appendix B for a description of the numerical model. One model run [panels (a), (c), and (e)] uses the average January 2017 stratification at the mid-latitude North Atlantic location (38° N, 45° W) [see the green 'x' in figure 4a] whereas the other [panels (b), (d), and (f)] uses the average July 2017 stratification at the same location. The stratification profiles are obtained from the Estimating the Circulation and Climate of the Ocean version 4 release 4 (ECCOV4, Forget et al. 2015) reanalysis product. Plots (a) and (b) show a snapshot of the surface potential vorticity at the ocean's surface in the January and July simulations respectively. Plots (c) and (d) show the resulting kinetic energy spectra along with the prediction in equation (50). Plots (e) and (f) show the spectral transfer functions Π_P , Π_E , and Π_K for surface potential enstrophy, total energy, and kinetic energy. These spectral transfer functions are normalized by their absolute maximum in plots (e) and (f) and are defined in the paragraph containing equation (24). If $\Pi_A > 0$, then the quantity A is cascading to smaller scales and conversely if $\Pi_A < 0$.

The contrast between the two simulations is evident in the surface potential vorticity snapshots of figure 1. In the January simulation [figure 1(a)], there are strong buoyancy gradients, small vortices alongside much larger ones, and there is evidence of large-scale strain. The July simulation 1(b)] lacks these features and appears diffuse in space.

c. The importance of variable stratification

Our main result is that the stratification's vertical structure controls both the dispersion of linear edge waves and the spatial locality of nonlinear interactions.

In turbulence with spatially non-local interactions, such as in two-dimensional vorticity dynamics, vortices induce

flows reaching far from the vortex core and the combined effects of distant vortices dominates the local fluid velocity. Thin, folding, potential vorticity filaments distinguish this spatially non-local turbulence. As the spatial non-locality is decreased (i.e., spatial locality increases), the dominance of large-scale strain weakens, and a secondary instability becomes possible in which filaments roll-up into small vortices (Pierrehumbert et al. 1994; Held et al. 1995). The resulting turbulence is distinguished by vortices spanning a wide range of scales, as in uniform stratification surface quasigeostrophic turbulence. Decreasing the spatial non-locality even further leads to vortices whose range is nearly limited to the vortex core; vortex mergers then appear like cell mitosis running backward in time (Polvani et al. 1989;

Larichev and McWilliams 1991). Large-scale strain is absent in these flows.

These qualitative changes in the turbulence accompany changes in the kinetic energy spectrum. Therefore, the dependence of the turbulence's spatial locality on the stratification provides a mechanism relating mixed-layer depth to the kinetic energy spectrum.

Deep wintertime mixed-layers result in turbulence that is more spatially non-local than the traditional constant stratification surface quasigeostrophic theory. For mid-latitude ocean parameters, the theory predicts a wintertime kinetic energy spectrum proportional to $k^{-7/3}$ in the forward cascade. This spectrum agrees with the January model simulation in figure 1(c).

In contrast, shallow summertime mixed-layers result in turbulence that is more spatially local and the theory predicts a shallower kinetic energy spectrum. However, the lack of scale invariance across the submesoscales in summertime turbulence results in the failure of the cascade theory. This failure of the summertime cascade theory can be seen in figure 1(d); the simulated spectrum is significantly steeper than the predicted spectrum, especially between 50-100 km. It is not clear what determines the slope of the summertime surface quasigeostrophic kinetic energy spectrum. Our simulations, which are only forced at large scales, indicate that the kinetic energy spectrum is steeper in winter than in summer at horizontal scales larger than 10 km. The simulations therefore imply a seasonality opposite to that observed in the ocean.

Therefore, variable stratification surface quasigeostrophic theory is seasonal—inheriting its seasonality from the stratification. Moreover, this seasonality is qualitatively consistent with certain aspects of oceanic submesoscale turbulence. Namely, the wintertime turbulence exhibits more fronts and vortices than summertime turbulence [compare our figure 1(a)-(b) with figure 1 in Sasaki et al. (2014) or Callies et al. (2015)]. We also find that the predicted vertical structure is consistent with the vertical structure of oceanic submesoscale turbulence. However, if we assume that the submesoscales are only forced at large-scales (as in figure 1), then we obtain a seasonal kinetic energy spectrum with a seasonality opposite to that of the oceanic submesoscales. It may be possible that accounting for (the seasonal) mixed-layer instability may result in a seasonality more consistent with observations. However, this suggestion is beyond the scope of this article.

d. Content of this paper

We begin the main part of this paper in section 2 by introducing the inversion function $m(k)$. The inversion function depends on the vertical stratification and it determines both linear wave dispersion and the turbulence's spatial locality. In section 3 we derive the cascade spectra in the forward and inverse cascade inertial ranges. These spectra depend

on the inversion function $m(k)$ and hence on the stratification. Section 4 then uses idealized stratification profiles to show that deep mixed-layers result in a spectral inversion relation whose spatial locality is halfway between two-dimensional turbulence and constant stratification surface quasigeostrophic theory. Section 5 uses reanalysis data to compute the inversion relation over the wintertime North Atlantic and finds that the spectral inversion relation indeed has this form. In section 6 we discuss the implied kinetic energy spectra in both summer and winter as well as the vertical structure of surface quasigeostrophic turbulence. We conclude in section 7.

2. The inversion function

a. Physical space equations

Consider an ocean of depth H with zero interior potential vorticity so that the geostrophic streamfunction satisfies

$$\nabla^2 \psi + \frac{\partial}{\partial z} \left(\frac{1}{\sigma^2} \frac{\partial \psi}{\partial z} \right) = 0 \quad \text{for } z \in (-H, 0). \quad (1)$$

In this equation, $\nabla^2 = \partial_x^2 + \partial_y^2$ is the horizontal Laplacian, ψ is the geostrophic streamfunction, and the inverse Prandtl ratio is

$$\sigma(z) = N(z)/f \quad (2)$$

where $N(z)$ is the depth-dependent buoyancy frequency and f is the constant local value of the Coriolis frequency. The horizontal geostrophic velocity is obtained from

$$\mathbf{u} = \hat{\mathbf{z}} \times \nabla \psi. \quad (3)$$

By an abuse of terminology, we refer to $\sigma(z)$ as *the stratification* for the remainder of the article.

The upper surface potential vorticity (with dimensions length per time) is given by (Bretherton 1966)

$$\theta = -\frac{1}{\sigma_0^2} \frac{\partial \psi}{\partial z} \Big|_{z=0}, \quad (4)$$

where $\sigma_0 = \sigma(0)$. The surface potential vorticity is related to the upper surface buoyancy anomaly, b , through $b = -f\sigma_0^2\theta$. The time-evolution equation at the upper boundary is

$$\frac{\partial \theta}{\partial t} + \mathbf{J}(\psi, \theta) + \Lambda \frac{\partial \psi}{\partial x} = F - D \quad \text{at } z = 0, \quad (5)$$

where $\mathbf{J}(\theta, \psi) = \partial_x \theta \partial_y \psi - \partial_y \theta \partial_x \psi$ represents the advection of θ by \mathbf{u} , F is the buoyancy forcing at the upper surface, and D is the dissipation. The frequency, Λ , appearing in equation (5) is defined by

$$\Lambda = \frac{1}{\sigma_0^2} \frac{dU}{dz} \quad (6)$$

where $U(z)$ is a background zonal geostrophic flow. Without loss of generality, we have assumed in equation (5) that $U(0) = 0$ to remove a constant advective term.

We assume a bottom boundary condition of

$$\psi \rightarrow 0 \text{ as } z \rightarrow -\infty \quad (7)$$

which is equivalent to assuming the bottom boundary is irrelevant to the dynamics. We will see that this assumption is valid in the mid-latitude open ocean for horizontal scales smaller than ≈ 500 km.

b. Fourier space equations

Assuming a doubly periodic domain in the horizontal prompts us to consider the Fourier expansion of ψ

$$\psi(\mathbf{r}, z, t) = \sum_{\mathbf{k}} \hat{\psi}_{\mathbf{k}}(t) \Psi_{\mathbf{k}}(z) e^{i\mathbf{k} \cdot \mathbf{r}} \quad (8)$$

where $\mathbf{r} = (x, y)$ is the horizontal position vector, $\mathbf{k} = (k_x, k_y)$ is the horizontal wavevector, and $k = |\mathbf{k}|$ is the horizontal wavenumber. The wavenumber dependent non-dimensional vertical structure, $\Psi_{\mathbf{k}}(z)$, is determined by the boundary-value problem¹

$$-\frac{d}{dz} \left(\frac{1}{\sigma^2} \frac{d\Psi_{\mathbf{k}}}{dz} \right) + k^2 \Psi_{\mathbf{k}} = 0 \quad (9)$$

with upper boundary condition

$$\Psi_{\mathbf{k}}(0) = 1 \quad (10)$$

and bottom boundary condition

$$\Psi_{\mathbf{k}} \rightarrow 0 \text{ as } z \rightarrow -\infty. \quad (11)$$

The upper boundary condition (10) is a normalization for the vertical structure, $\Psi_{\mathbf{k}}(z)$, chosen so that

$$\psi(\mathbf{r}, z=0, t) = \sum_{\mathbf{k}} \hat{\psi}_{\mathbf{k}}(t) e^{i\mathbf{k} \cdot \mathbf{r}}. \quad (12)$$

Consequently, the surface potential vorticity (4) is given by

$$\theta(\mathbf{r}, t) = \sum_{\mathbf{k}} \hat{\theta}_{\mathbf{k}}(t) e^{i\mathbf{k} \cdot \mathbf{r}} \quad (13)$$

where

$$\hat{\theta}_{\mathbf{k}} = -m(k) \hat{\psi}_{\mathbf{k}} \quad (14)$$

¹To derive equation (9), substitute the Fourier representation (8) into equation (1), multiply by $e^{-i\mathbf{l} \cdot \mathbf{r}}$, take an area average, and use the identity

$$\frac{1}{A} \int_A e^{i(\mathbf{k}-\mathbf{l}) \cdot \mathbf{r}} d\mathbf{r} = \delta_{\mathbf{k}, \mathbf{l}}$$

where $\delta_{\mathbf{k}, \mathbf{l}}$ is the Kronecker delta, and A is the horizontal area of the periodic domain.

and the inversion function (with dimensions of inverse length) $m(k)$ is defined as

$$m(k) = \frac{1}{\sigma_0^2} \frac{d\Psi_{\mathbf{k}}(0)}{dz}. \quad (15)$$

In all our applications, the inversion function $m(k)$ is a positive increasing function of k (i.e., $m(k) > 0$ and $dm/dk > 0$). However, we have no mathematical proofs of these properties.

The inversion function determines the spectral inversion relation (14) between the surface potential vorticity and streamfunction, and hence it characterizes the dynamics of the surface quasigeostrophic fluid. For example, the edge wave frequency is given by

$$\omega(\mathbf{k}) = -\frac{\Lambda k_x}{m(k)} \quad (16)$$

which shows that the dispersion of edge waves depends on the functional form of the inversion function [and therefore on the stratification $\sigma(z)$].

In addition, the inversion function is related to the turbulence's spatial locality (as discussed in section 1c) in the following manner. A steep inversion function implies a spatially non-local flow dominated by strain; for example, an inversion function $m(k) \sim k^2$ implies dynamics analogous to two-dimensional vorticity dynamics [we do not find inversion functions steeper than $m(k) \sim k^2$]. The inversion function is less steep in constant stratification surface quasigeostrophic theory, with $m(k) \sim k$. In this case, straining due to distant eddies is less important and the resulting turbulence is more local in space. In sections 4 and 5, we find an inversion function $m(k) \sim k^{3/2}$ implying a spatial locality halfway between two-dimensional vorticity dynamics and constant stratification surface quasigeostrophic dynamics. Finally, as the inversion function becomes very flat ($dm/dk \rightarrow 0$), we obtain dynamics that are highly local in space, analogous to the regime described in Larichev and McWilliams (1991).

c. The case of constant stratification

To recover the well-known case of constant stratification surface quasigeostrophic theory (Blumen 1978; Held et al. 1995), set $\sigma = \sigma_0$. Then equation (9) along with boundary conditions (10) and (11) yield the exponentially decaying vertical structure, $\Psi_{\mathbf{k}}(z) = e^{\sigma_0 k z}$. Substituting $\Psi_{\mathbf{k}}(z)$ into equation (15) then gives $m(k) = k/\sigma_0$ and hence a linear-in-wavenumber inversion relation of $\hat{\theta}_{\mathbf{k}} = -(k/\sigma_0) \hat{\psi}_{\mathbf{k}}$.

3. Surface quasigeostrophic turbulence

Suppose a two-dimensional fluid is forced in the wavenumber interval $[k_1, k_2]$. In such a fluid, Kraichnan (1967) argues that two inertial ranges will form: one

inertial range for $k < k_1$ where kinetic energy cascades to larger scales and another inertial range for $k > k_2$ where enstrophy cascades to smaller scales. Kraichnan's argument depends on three properties of two-dimensional vorticity dynamics. First, that there are two independent conserved quantities; namely, the kinetic energy and the enstrophy. Second, that turbulence is sufficiently local in wavenumber space so that the only available length scale is k^{-1} . Third, that the inversion relation between vorticity and the streamfunction is scale invariant.

There are two independent conserved quantities in surface quasigeostrophic dynamics, as in Kraichnan's two-dimensional fluid. For the cases considered here, with non-constant $m(k)$, the conserved quantities are the total energy, E , and the surface potential enstrophy, P . However, the second and third properties of two-dimensional vorticity dynamics do not hold for surface quasigeostrophic dynamics. Even if the turbulence is local in wavenumber space, there are two available length scales at each wavenumber k ; namely, k^{-1} and $[m(k)]^{-1}$. Moreover, the inversion relation (14) is generally not scale invariant.² Therefore, the arguments in Kraichnan (1967) do not hold in general for surface quasigeostrophic dynamics.

Even so, in the remainder of this section we show that there is a net inverse cascade of total energy and a net forward cascade of surface potential enstrophy even if there are no inertial ranges in the turbulence. Then we consider the circumstances under which we expect inertial ranges to form. Finally, assuming the existence of an inertial range, we derive the spectra for the cascading quantities. We begin, however, with some definitions.

a. Quadratic quantities

The two quadratic quantities needed for the cascade argument are the volume-integrated total energy per mass per unit area E ,

$$\begin{aligned} E &= \frac{1}{2A} \int_V \left(|\nabla \psi|^2 + \frac{1}{\sigma^2} \left| \frac{\partial \psi}{\partial z} \right|^2 \right) dV \\ &= -\frac{1}{2} \overline{\psi|_{z=0} \theta} = \frac{1}{2} \sum_k m(k) |\hat{\psi}_k|^2 \end{aligned} \quad (17)$$

and the upper surface potential enstrophy,

$$P = \frac{1}{2} \overline{\theta^2} = \frac{1}{2} \sum_k [m(k)]^2 |\hat{\psi}_k|^2 \quad (18)$$

where the overline denotes an area average over the periodic domain. Both quantities are conserved in the absence of

forcing and dissipation, as can be seen by multiplying the time-evolution equation (5) by either $-\psi|_{z=0}$ or θ and taking an area average.

Two other quadratics we use are the surface kinetic energy

$$K = \frac{1}{2} \overline{|\nabla \psi|_{z=0}^2} = \frac{1}{2} \sum_k k^2 |\hat{\psi}_k|^2 \quad (19)$$

and the surface streamfunction variance

$$S = \frac{1}{2} \overline{(\psi|_{z=0})^2} = \frac{1}{2} \sum_k |\hat{\psi}_k|^2. \quad (20)$$

The isotropic spectrum $\mathcal{A}(k)$ of a quantity A is defined by

$$A = \int_0^\infty \mathcal{A}(k) dk, \quad (21)$$

so that the isotropic spectra of E, P, K , and S are given by $\mathcal{E}(k), \mathcal{P}(k), \mathcal{K}(k)$, and $\mathcal{S}(k)$. The isotropic spectra are then related by

$$\mathcal{P}(k) = m(k) \mathcal{E}(k) = [m(k)]^2 \mathcal{S}(k) \quad (22)$$

and

$$\mathcal{K}(k) = k^2 \mathcal{S}(k). \quad (23)$$

For each spectral density $\mathcal{A}(k)$, there is a time-evolution equation of the form (e.g., Gkioulekas and Tung 2007)

$$\frac{\partial \mathcal{A}(k)}{\partial t} + \frac{\partial \Pi_A(k)}{\partial k} = F_A(k) - D_A(k) \quad (24)$$

where $\Pi_A(k)$ is transfer of the spectral density $\mathcal{A}(k)$ from $(0, k)$ to (k, ∞) , and $D(k)$ and $F(k)$ are the dissipation and forcing spectra of A , respectively. In an inertial range where A is the cascading quantity, then $\Pi_A(k) = \varepsilon_A$ where ε_A is a constant and thus $\partial \Pi_A(k)/\partial k = 0$.

b. The inverse and forward cascade

For a fluid with a spectral inversion relation of the form given by equation (14) that is forced in wavenumber interval $[k_1, k_2]$, Gkioulekas and Tung (2007) prove the following two inequalities for stationary turbulence,

$$\int_0^k \frac{dm(k')}{dk'} \Pi_E(k') dk' < 0, \text{ for all } k > k_2, \quad (25)$$

$$\int_k^\infty \frac{dm(k')}{dk'} \frac{\Pi_P(k')}{[m(k')]^2} dk' > 0, \text{ for all } k < k_1. \quad (26)$$

These two inequalities do not require the existence of inertial ranges—only that the inversion function $m(k)$ is an increasing function of k . Therefore, if $dm(k)/dk > 0$, which holds for all cases considered in this paper, then there is a net inverse cascade of total energy E and a net forward cascade of total surface potential enstrophy P .

² A function $m(k)$ is scale invariant if $m(\lambda k) = \lambda^s m(k)$ for all λ , where s is a real number. Power laws $m(k) = k^\alpha$ are scale invariant. It follows then that both two-dimensional vorticity dynamics and constant stratification surface quasigeostrophic dynamics have scale invariant spectral inversion relations.

c. *When do inertial ranges form?*

The lack of scale invariance along with the presence of two length scales, k^{-1} and $[m(k)]^{-1}$, prevents the use of the Kraichnan (1967) argument to establish the existence of an inertial range. However, suppose that in a wavenumber interval $[k_a, k_b]$ the inversion function takes the form of a power law

$$m(k) \approx m_0 k^\alpha, \quad (27)$$

where $m_0 > 0$ and $\alpha > 0$. We then define the α -vorticity $\theta^{(\alpha)}$ by $\theta^{(\alpha)} = \theta/m_0$ so that the inversion relation for $k \in [k_a, k_b]$ becomes

$$\hat{\theta}_k^{(\alpha)} \approx -k^\alpha \hat{\psi}_k. \quad (28)$$

With this transformation, then in the wavenumber interval $[k_a, k_b]$, the inversion relation (28) is scale invariant. Moreover, k^{-1} is the only available length scale if the turbulence is sufficiently local in wavenumber space.

It follows that if the wavenumber interval $[k_a, k_b]$ is sufficiently wide (i.e., $k_a \ll k_b$), then Kraichnan's argument applies to the turbulence over this wavenumber range. Indeed, two-dimensional fluids with an inversion relation of the form (28) have been investigated by Pierrehumbert et al. (1994). They provide expressions for the spectra of the cascading quantities, which we generalize below.

d. *The Tulloch and Smith (2006) argument*

If we assume the existence of inertial ranges, we can adapt the cascade argument of Tulloch and Smith (2006) to general surface quasigeostrophic fluids to obtain predictions for the cascade spectra.

In the inverse cascade inertial range, we must have $\Pi_E(k) = \varepsilon_E$ where ε_E is a constant. Assuming locality in wavenumber space, we have

$$\varepsilon_E \sim \frac{k \mathcal{E}(k)}{\tau(k)} \quad (29)$$

where $\tau(k)$ is a spectrally local timescale.

Several spectrally local timescales are available. We have the kinetic energy timescale,

$$\tau_K(k) \sim [k^3 \mathcal{K}(k)]^{-1/2}, \quad (30)$$

the total energy timescale,

$$\tau_E(k) \sim [k^4 \mathcal{E}(k)]^{-1/2}, \quad (31)$$

and the surface potential enstrophy timescale

$$\tau_P(k) \sim [k^3 \mathcal{P}(k)]^{-1/2}. \quad (32)$$

Once a quantity A has been chosen, the timescale $\tau_A(k)$ is determined by dimensional analysis.

Assuming that $\tau(k) = \tau_K(k)$, then substituting the timescale into equation (29) and using the relationship between the energy spectrum $\mathcal{E}(k)$ and the streamfunction variance spectrum $\mathcal{K}(k)$ in equations (22) and (23), we obtain the total energy spectrum in the inverse cascade inertial range

$$\mathcal{E}(k) \sim \varepsilon_E^{2/3} k^{-7/3} [m(k)]^{1/3}. \quad (33)$$

Analogously, in the forward cascade inertial range, we must have $\Pi_P(k) = \varepsilon_P$ where ε_P is a constant. A similar argument yields the surface potential enstrophy spectrum in the forward cascade inertial range

$$\mathcal{P}(k) \sim \varepsilon_P^{2/3} k^{-7/3} [m(k)]^{2/3}. \quad (34)$$

The predicted spectra (33) and (34) are not uniquely determined by dimensional analysis. Rather than assuming that the spectrally local timescale $\tau(k)$ is determined by the kinetic energy spectrum $\mathcal{K}(k)$, we can assume that $\tau(k) = \tau_E(k)$ or $\tau(k) = \tau_P(k)$. Either choice will result in cascade spectra distinct from (33) and (34). However, by assuming that the timescale $\tau(k) = \tau_K(k)$, the resulting cascade spectra agree with the α -turbulence predictions of Pierrehumbert et al. (1994) when the inversion function takes the power law form (27).

e. *Summary of the turbulence theory*

To summarize, we are not able to establish the general existence of inertial ranges. Nevertheless, the Gkioulekas and Tung (2007) inequalities, equations (25) and (26), show that there must be a net inverse total energy cascade and a net forward surface potential enstrophy cascade in surface quasigeostrophic turbulence. These inequalities only assume that $dm(k)/dk > 0$.

Moreover, if the inversion function takes the power law form (27) over a sufficiently wide wavenumber interval, we expect the α -turbulence theory of Pierrehumbert et al. (1994) to hold. In this wavenumber interval, the appropriate inertial range will form and the resulting cascade spectra are given by equations (33) and (34).

Finally, if we assume the existence of an inertial range and that the spectrally local timescale, $\tau(k)$, is determined by the kinetic energy spectrum, $\mathcal{K}(k)$, then we obtain the cascade spectra (33) and (34). However, the validity of these spectra is uncertain when the inversion function is not a power law. When the inversion function is not a power law, the cascade spectra (33) and (34) may fail either because no inertial range exists or because the spectrally local time scale is not determined by the kinetic energy spectrum, $\mathcal{K}(k)$.

4. Idealized stratification profiles

a. An idealized mixed-layer

We now present an idealized stratification profile, $\sigma(z) = N(z)/f$, for which the inversion function, $m(k)$, displays a $k^{3/2}$ dependence at the submesoscales. Such an inversion function implies a spatial locality halfway between constant stratification surface quasigeostrophic dynamics and two-dimensional vorticity dynamics.

Consider the piecewise stratification profile given by

$$\sigma(z) = \begin{cases} \sigma_0 & \text{for } -h_{\text{mix}} < z \leq 0 \\ \sigma_0 + \Delta\sigma \left(\frac{z+h_{\text{mix}}}{h_{\text{lin}}} \right) & \text{for } -(h_{\text{mix}} + h_{\text{lin}}) < z \leq -h_{\text{mix}} \\ \sigma_{\text{pyc}} & \text{for } z \leq -(h_{\text{mix}} + h_{\text{lin}}) \end{cases} \quad (35)$$

where

$$\Delta\sigma = \sigma_0 - \sigma_{\text{pyc}}. \quad (35)$$

This stratification profile consists of an upper layer of thickness, h_{mix} , with constant stratification, σ_0 . Below, for depths between h_{mix} and $h_{\text{mix}} + h_{\text{lin}}$, is a linearly stratified region of thickness h_{lin} . Finally, at a depth of $-(h_{\text{mix}} + h_{\text{lin}})$ is an infinitely deep layer of constant stratification, σ_{pyc} . If $\sigma_0 < \sigma_{\text{pyc}}$ (so that $\Delta\sigma < 0$) then this stratification profile is an idealization of a weakly stratified mixed-layer overlying an ocean of stronger stratification, σ_{pyc} , with a linear transition layer in between. See panels (b) and (e) in figure 2 for an illustration.

There are two horizontal length scales arising from this stratification profile. The mixed-layer length scale is given by

$$L_{\text{mix}} = 2\pi\sigma_0 h_{\text{mix}}. \quad (36)$$

At horizontal scales smaller than L_{mix} , we expect the inversion function $m(k)$ to have the form $m(k) \approx k/\sigma_0$ as in constant stratification surface quasigeostrophic theory. The second length scale is the pycnocline length scale

$$L_{\text{pyc}} = 2\pi\sigma_{\text{pyc}} (h_{\text{mix}} + h_{\text{lin}}). \quad (37)$$

At horizontal scales much larger than L_{pyc} , we expect the inversion function $m(k)$ to have the form $m(k) \approx k/\sigma_{\text{pyc}}$ because at large horizontal scales, the ocean will seem to have constant stratification σ_{pyc} . This large scale limit, however, is not realistic because the ocean is not infinitely deep nor does the ocean have constant stratification below the pycnocline.

If we assume that $m(k)$ is a continuous function, then it must transition between these two limiting forms at the horizontal scales given by

$$L_{\text{mix}} < \frac{2\pi}{k} < L_{\text{pyc}}. \quad (38)$$

Our aim in this section is to uncover the functional dependence of the inversion function $m(k)$ on the wavenumber k at these intermediate length scales.

1) THE SHARP TRANSITION LIMIT

We first consider the limit $h_{\text{lin}} \ll h_{\text{mix}}$ for which the stratification jumps from a surface value of σ_0 to a deep ocean value of σ_{pyc} at $z = -h_{\text{mix}}$,

$$\sigma(z) \approx \begin{cases} \sigma_0 & \text{for } -h_{\text{mix}} < z \leq 0 \\ \sigma_{\text{pyc}} & \text{for } z \leq -h_{\text{mix}}. \end{cases} \quad (39)$$

In this limit an analytical solution is possible, with the solution provided in appendix A. The resulting inversion function is

$$m(k) \approx \frac{k}{\sigma_0} \left[\frac{\cosh(\sigma_0 h_{\text{mix}} k) + \left(\frac{\sigma_{\text{pyc}}}{\sigma_0} \right) \sinh(\sigma_0 h_{\text{mix}} k)}{\sinh(\sigma_0 h_{\text{mix}} k) + \left(\frac{\sigma_{\text{pyc}}}{\sigma_0} \right) \cosh(\sigma_0 h_{\text{mix}} k)} \right].$$

As expected, the small scale limit is $m(k) \approx k/\sigma_0$ whereas the large scale limit is $m(k) \approx k/\sigma_{\text{pyc}}$. We now examine two limiting cases.

If $\sigma_0 \ll \sigma_{\text{pyc}}$, that is, if a weakly stratified mixed-layer overlies a strongly stratified deep ocean, then we obtain

$$m(k) \approx \frac{k}{\sigma_0} \tanh(\sigma_0 h k) \quad (40)$$

which at large horizontal scales becomes proportional to a square power law. However, this regime is only valid at the intermediate scales, given by equation (38), so we only expect a steepening of the inversion function $m(k)$ to have a super-linear k -dependence.

Figure 2 (a)-(c) presents an example. The stratification $\sigma(z)$ abruptly jumps from a surface value of $\sigma_0 \approx 14$ to a value of $\sigma_{\text{pyc}} = 100$ at a depth of $z = -h_{\text{mix}} = -100$ m. At both horizontal scales smaller than $L_{\text{mix}} \approx 10$ km and at horizontal scales much larger than $L_{\text{pyc}} \approx 70$ km, the inversion function is linear. However, at horizontal length scales between L_{mix} and L_{pyc} the inversion function has the approximate form $m(k) \sim k^{1.6}$.

The second case is that of a strongly stratified upper ocean overlying a weakly stratified deep ocean, that is, when $\sigma_0 \gg \sigma_{\text{pyc}}$. In this case we obtain

$$m(k) \approx \frac{k}{\sigma_0} \coth(\sigma_0 h k) \quad (41)$$

which at large horizontal scales becomes constant. We therefore expect a relatively flat inversion function, $m(k)$, with a sub-linear k -dependence. Although we do not consider this case further, this case is similar to that of an exponential stratification profile, which we consider in section 4b.

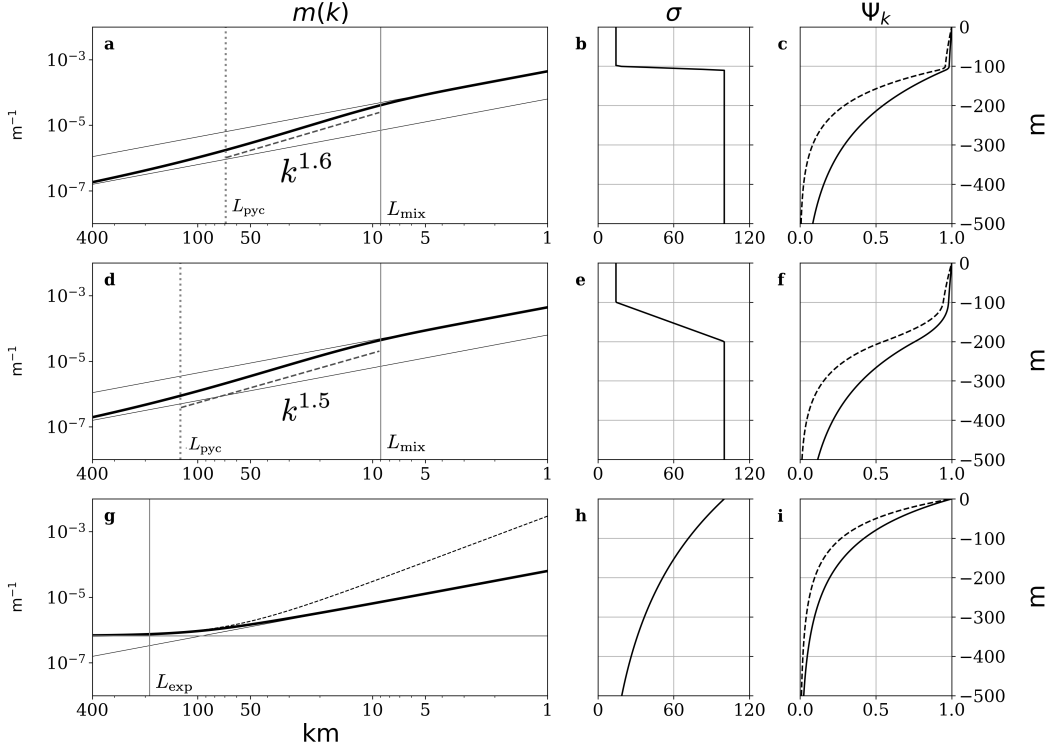


FIG. 2. Log-log plots of the inversion function $m(k)$ [panels (a), (d), and (g)], for three stratification profiles [panels (b), (e), and (h)] and the resulting streamfunctions at the two horizontal length scales of 50 km (dashed) and 100 km (solid) [panels (c), (f), and (i)]. In the first two inversion function plots [panels (a) and (d)], the thin solid diagonal lines represent the two linear asymptotic states of k/σ_0 and k/σ_{pyc} . The vertical solid line is the mixed-layer length scale L_{mix} , given by equation (36), whereas the vertical dotted line is the pycnocline length scale L_{pyc} , given by equation (37). The power α , where $m(k)/k^\alpha \approx \text{constant}$, is computed by fitting a straight line to the log-log plot of $m(k)$ between $2\pi/L_{\text{mix}}$ and $2\pi/L_{\text{pyc}}$. This straight line is shown as a grey dashed line in panels (a) and (d). In panel (g), the thin grey lines are the linear small-scale limit, $m(k) \approx k/\sigma_0$, and the constant large-scale limit, $m(k) \approx 2/(\sigma_0^2 h_{\text{exp}})$. The dashed line is the large-scale limit with the higher order quadratic term, given by equation (46). Finally, the solid vertical line in panel (g) is the horizontal length scale L_{exp} (43) induced by the exponential stratification. Further details on the stratification profiles are in the text.

2) THE GENERAL CASE

If we consider h_{lin} to be the thickness of the vertical region bounded above by the bottom of the mixed-layer and bounded below by the depth of the maximum pycnocline stratification, then h_{lin} is typically not much smaller than h_{mix} . That is, the sharp transition limit of $h_{\text{lin}} \ll h_{\text{mix}}$ is not valid and so we must consider the general case with a finite h_{lin} .

As shown in figure 2, a finite h_{lin} extends the width of the intermediate regime (38). Because the inversion function $m(k)$ must transition from the same asymptotic limits of k/σ_0 to k/σ_{pyc} over a wider range of intermediate scales (38), we expect a shallower slope than the $h_{\text{lin}} \ll h_{\text{mix}}$ case, which is indeed what is found.

We have seen in figure 2 that $m(k)$ can be approximated as a power law, $m(k) \sim k^\alpha$, at the intermediate scales (38). In figure 3 we show how the power α depends on the ratios $h_{\text{lin}}/h_{\text{mix}}$ and $\sigma_{\text{pyc}}/\sigma_0$. Typical wintertime values

are $\sigma_{\text{pyc}}/\sigma_0 \approx 5 - 15$ and $h_{\text{lin}}/h_{\text{mix}} \approx 0.3 - 1$ which imply $\alpha \approx 1.5 - 1.6$.

As expected, figure 3 shows that larger $h_{\text{lin}}/h_{\text{mix}}$ tend to decrease α due to the widening of the intermediate scales of equation (38). Figure 3 also shows that a larger stratification ratio $\sigma_{\text{pyc}}/\sigma_0$ results in a larger α and hence a steeper inversion function, $m(k)$.

b. An exponentially stratified ocean

Now consider an exponential stratification profile

$$\sigma = \sigma_0 e^{z/h_{\text{exp}}}. \quad (42)$$

The form of $\sigma(z)$ introduces the vertical scale, h_{exp} , which in turn yields a horizontal scale

$$L_{\text{exp}} = 2\pi \sigma_0 h_{\text{exp}}. \quad (43)$$

Substituting (42) into vertical structure equation (9) with boundary condition (10) and (11) yields the vertical struc-

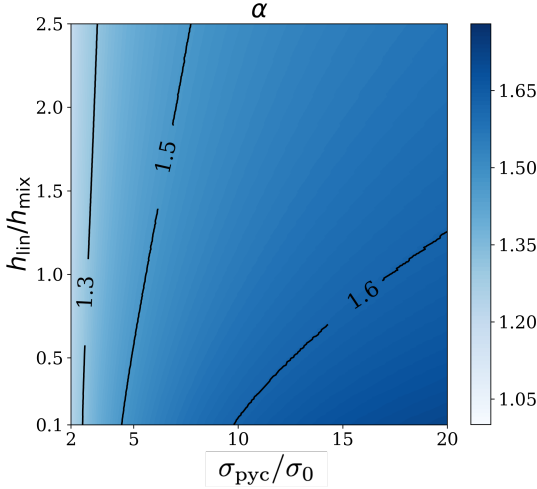


FIG. 3. A plot of α , where $m(k)/k^\alpha \approx \text{const}$, at the intermediate horizontal scales given by equation (38) for a mixed-layer like stratification $\sigma(z)$ given by the unnumbered equation immediately preceding equation (35). The power α is obtained by fitting a straight line to a log-log plot of $m(k)$ between $2\pi/L_{\text{mix}}$ and $2\pi/L_{\text{pyc}}$ (as in figure 2). We fix $h_{\text{lin}} = 50$ m and $\sigma_{\text{pyc}} = 100$ in the calculation. Typical wintertime values are $\sigma_{\text{pyc}}/\sigma_0 \approx 5 - 15$ and $h_{\text{lin}}/h_{\text{mix}} \approx 0.3 - 1$.

ture

$$\Psi_k(z) = e^{z/h_{\text{exp}}} \frac{I_1(e^{z/h_{\text{exp}}} \sigma_0 h_{\text{exp}} k)}{I_1(\sigma_0 h_{\text{exp}} k)} \quad (44)$$

where $I_n(z)$ is the modified Bessel function of the first kind of order n .

To obtain the inversion function, substitute the vertical structure (44) into the definition of the inversion function (15) to obtain

$$m(k) = \frac{1}{\sigma_0^2 h_{\text{exp}}} + \frac{k}{2\sigma_0} \left[\frac{I_0(\sigma_0 h_{\text{exp}} k)}{I_1(\sigma_0 h_{\text{exp}} k)} + \frac{I_2(\sigma_0 h_{\text{exp}} k)}{I_1(\sigma_0 h_{\text{exp}} k)} \right]. \quad (45)$$

In the small-scale limit $k \gg 2\pi/L_{\text{exp}}$, equation (45) becomes $m(k) \approx k/\sigma_0$ as in constant stratification surface quasigeostrophic theory. In contrast, the large-scale limit $k \ll 2\pi/L_{\text{exp}}$ gives

$$m(k) \approx \frac{2}{\sigma_0^2 h_{\text{exp}}} + \frac{h_{\text{exp}} k^2}{4} \quad (46)$$

which is approximately constant to leading order in k .

Figure 2(g)-(i) shows a case with $\sigma_0 = 100$ and $h_{\text{exp}} = 300$ m. For horizontal scales larger than 50 km, the large scale approximation (46) with the higher order quadratic term holds. At scales smaller than 50 km, the inversion function rapidly transitions to the linear small scale limit

of $m(k) \approx k/\sigma_0$. In contrast, for realistic stratification profiles, we will see that the transition is more gradual, occurring over a wide range of wavenumbers. Moreover, the bottom boundary condition becomes important before the large scale limit (46) is reached.

5. Application to the ECCOV4 ocean state estimate

We now show that over the mid-latitude Atlantic, the inversion function $m(k)$ has the approximate form $m(k) \sim k^{3/2}$ at the submesoscales in winter. To compute the inversion function $m(k)$, we obtain the stratification profile $\sigma(z) = N(z)/f$ at each location from the Estimating the Circulation and Climate of the Ocean version 4 release 4 (ECCOV4, Forget et al. 2015) reanalysis product. We then compute $\Psi_k(z)$ using the vertical structure equation (9) and use equation (15) to obtain the inversion function $m(k)$ at each wavenumber k .

a. The three horizontal length-scales

In addition to L_{mix} and L_{pyc} [defined in equations (36) and (37)], we introduce the horizontal length scale, L_H , the full-depth horizontal scale, defined by

$$L_H = 2\pi \sigma_{\text{ave}} H, \quad (47)$$

where σ_{ave} is the vertical average of σ and H is the ocean depth. The bottom boundary condition becomes important to the dynamics at horizontal scales larger than $\approx L_H$.

We compute all three length scales using ECCOV4 stratification profiles over the North Atlantic, with results displayed in figure 4(a)-(c). To compute the mixed-layer horizontal scale $L_{\text{mix}} = 2\pi\sigma_0 h_{\text{mix}}$, we set σ_0 equal to the stratification at the uppermost grid cell. The mixed-layer depth h_{mix} is then defined as follows. We first define the pycnocline stratification σ_{pyc} to be the maximum of $\sigma(z)$. The mixed-layer depth h_{mix} is then the depth at which $\sigma(-h_{\text{mix}}) = \sigma_0 + (\sigma_{\text{pyc}} - \sigma_0)/4$. Finally, the pycnocline horizontal scale L_{pyc} is computed as $L_{\text{pyc}} = 2\pi\sigma_{\text{pyc}} h_{\text{pyc}}$ where h_{pyc} is the depth of the stratification maximum σ_{pyc} .

Figure 4(a) shows that typical values of L_H over the mid-latitude open ocean range between 400 – 700 km. On continental shelves, as well as high-latitudes, L_H decreases to values smaller than 200 km. As we approach the equator the full-depth horizontal scale L_H becomes large due to the smallness of the Coriolis parameter.

Constant stratification surface quasigeostrophic theory is only relevant for horizontal scales smaller than L_{mix} . Figure 4(b) shows that L_{mix} is spatially variable with wintertime values ranging between 1 – 15 km.

The pycnocline horizontal scale indicates the large-scale limit of the wintertime $m(k) \sim k^{3/2}$ regime. Figure 4(c) shows that typical mid-latitude values range between 70 – 110 km.

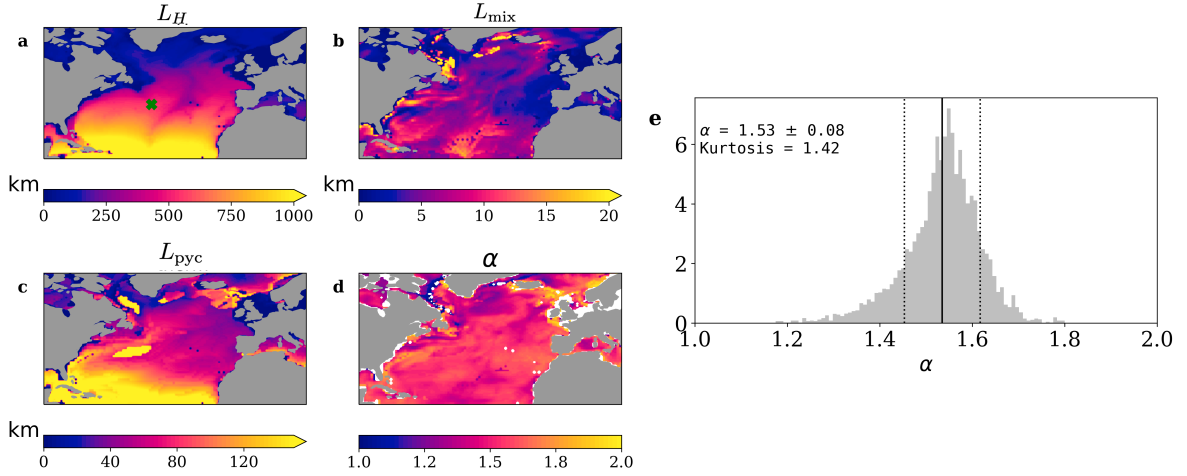


Fig. 4. Panels (a), (b), and (c) show the horizontal length scales L_H , L_{mix} , and L_{pyc} as computed from ECCOV4 stratification profiles, $\sigma(z) = N(z)/f$, over the North Atlantic. The green ‘x’ in panel (a) shows the location chosen for the model simulations of figure 1 and 6, as well as for the inversion functions of figure 5. Panel (d) shows α , defined by $m(k)/k^\alpha \approx \text{constant}$, over the North Atlantic. We compute α by fitting a straight line to a log-log plot of $m(k)$ between $2\pi/L_{\text{mix}}$ and $2\pi/L_{\text{pyc}}$. Panel (e) is a histogram of the computed values of α over the North Atlantic. We exclude from this histogram areas with $L_H < 150$ km; these are primarily continental shelves and high-latitude regions. In these excluded regions, our chosen bottom boundary condition (48) may be influencing the computed value of α .

b. The inversion function $m(k)$ at a single location.

Before computing the form of the inversion function $m(k)$ over the North Atlantic, we focus on a single location.

We must first address what boundary conditions to use in solving equation (9) for the vertical structure $\Psi_k(z)$. Although we can use upper boundary condition (10), we cannot use the infinite bottom boundary condition (11) because the ocean has a finite depth. However, given that figure 4(a) shows that the bottom boundary condition should not effect the inversion function for horizontal scales smaller than 400 km in the mid-latitude open ocean, we choose to use the homogeneous Dirichlet bottom boundary condition

$$\Psi_k(-H) = 0. \quad (48)$$

The alternate homogeneous Neumann boundary condition

$$\frac{d\Psi_k(-H)}{dz} = 0 \quad (49)$$

gives qualitatively identical results for the scales smaller than 400 km, which are the scales of interest in this study.

Figure 5 shows the computed inversion function in the mid-latitude North Atlantic at (38° N, 45° W) [see the green ‘x’ in figure 4(a)]. In January, at horizontal scales smaller than approximately $L_{\text{mix}} \approx 5$ km, we recover the linear $m(k) \approx k/\sigma_0$ expected from constant stratification surface quasigeostrophic theory. However, for horizontal scales between $L_{\text{mix}} \approx 5$ km and $L_{\text{pyc}} \approx 70$ km, the inversion function $m(k)$ has an approximate $k^{3/2}$ dependence.

In summer, the mixed-layer horizontal scale L_{mix} becomes smaller than 1 km while the pycnocline horizontal scale L_{pyc} decreases to 20 km. We thus obtain an $m(k) \sim k^{1.2}$ regime, but only for horizontal scales between 1-20 km. Thus, although there is a range of wavenumbers for which $m(k)$ steepens to a super-linear k -dependence in summer, this range of wavenumbers is narrow, only found at small scales, and the steepening is much less pronounced than in winter.

At scales between L_{pyc} and L_H , another inversion function regime emerges that is especially prominent in summer. Namely, the exponential nature of ocean stratification below the pycnocline leads the inversion function $m(k)$ to flatten between L_{pyc} and L_H to a sub-linear k -dependence. However, the inversion function in this regime does not generally display an approximate power law behavior.

c. The inversion function over the North Atlantic

We now present the form of the inversion function $m(k)$ for horizontal scales between L_{mix} and L_{pyc} over the North Atlantic. We obtain the power α , where $m(k)/k^\alpha \approx \text{constant}$, by fitting a straight line to $m(k)$ on a log-log plot between $2\pi/L_{\text{mix}}$ and $2\pi/L_{\text{pyc}}$. A value of $\alpha = 1$ is expected for constant stratification surface quasigeostrophic theory. A value of $\alpha = 2$ leads to an inversion relation similar to two-dimensional vorticity dynamics. In general, larger values of α lead to increased spatial non-locality and indicate a larger role for large-scale strain (Pierrehumbert et al. 1994).

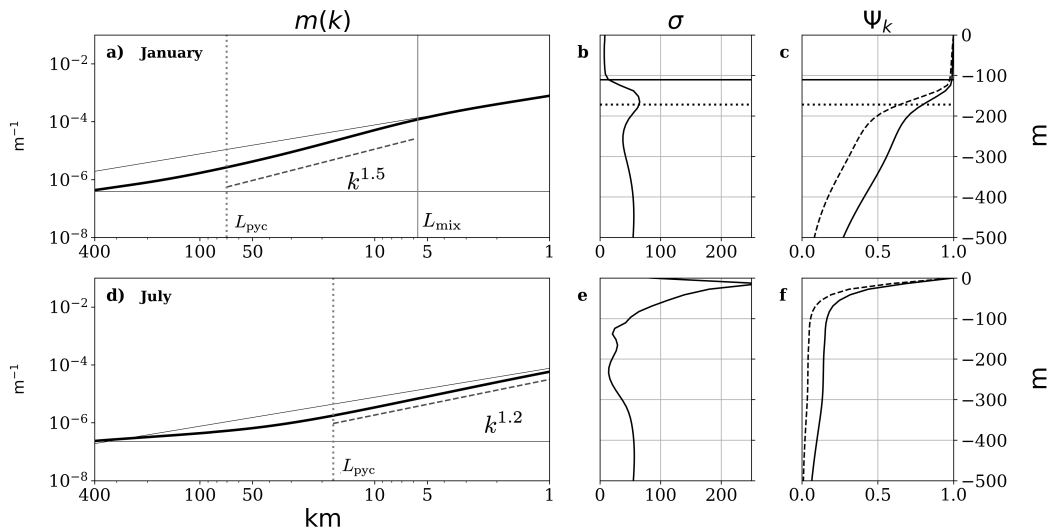


FIG. 5. As in figure 2 but for the mid-latitude North Atlantic location (38° N , 45° W) in January [(a)-(c)] and July [(d)-(f)]. This location is marked by a green ‘x’ in figure 4(a). In plots (b) and (c), the solid horizontal line represents $z = -h_{\text{mix}}$ and the dotted horizontal line represents $z = -h_{\text{pyc}}$. Only the upper 500 m of the stratification profiles and vertical structure are shown in panels (b), (c), (e) and (f).

Figure 4(d) shows that we generally have $\alpha \approx 3/2$ in the open ocean. There appears to be some deviations at high-latitudes (e.g., the Labrador sea and southeast of Greenland) and on continental shelves where we find regions of low α . However, both of these regions have small value of L_H so that our chosen bottom boundary condition (48) can be influencing the computed α there.

A histogram of the computed values of α [figure 4(e)] confirms that $\alpha \approx 1.53 \pm 0.08$ in the wintertime mid-latitude open ocean. This histogram only includes grid cells with $L_H > 150 \text{ km}$, which ensures that our chosen bottom boundary condition (48) is not influencing the computed distribution.

The universality of the $m(k) \sim k^{3/2}$ regime over the mid-latitudes is expected because it depends on a mechanism universally present over the mid-latitude ocean in winter; namely, the deepening of the mixed-layer. However, a comment is required on why this regime also appears at low-latitudes where we do not observe deep wintertime mixed-layers. At low-latitudes, the $m(k) \sim k^{3/2}$ regime emerges because there is a large scale-separation between L_{mix} and L_{pyc} . The smallness of the low-latitude Coriolis parameter f cancels out the shallowness of the low-latitude mixed-layer depth resulting in values of L_{mix} comparable to the remainder of the mid-latitude Atlantic, as seen in figure 4(b). However, no similar cancellation is observed for L_{pyc} which reaches values of $\approx 500 \text{ km}$ due to the smallness of the Coriolis parameter f at low-latitudes. This results in a non-seasonal $m(k) \sim k^{3/2}$ regime at low-latitudes for horizontal scales between 10 – 500 km.

6. Discussion

We now discuss whether the theory can account for the three discrepancies between the constant stratification surface quasigeostrophic theory and submesoscale dynamics listed in the introduction. It is clear that surface quasigeostrophic turbulence is seasonal through its dependence on the stratification. What is unclear is whether this seasonality corresponds to what is found at the ocean submesoscales. We therefore begin with the failure of the cascade theory in summer. We then address the wintertime kinetic energy spectrum and its relation to mixed-layer baroclinic instability. Afterwards, we discuss the vertical structure of surface quasigeostrophic turbulence. Finally, we relate our article to previous articles on surface quasigeostrophic dynamics with variable stratification.

a. Failure of the cascade theory in summer

The kinetic energy spectrum in the forward cascade inertial range is derived using equations (22), (23), and (34),

$$\mathcal{K}(k) \sim \varepsilon_P^{2/3} k^{-1/3} [m(k)]^{-4/3}. \quad (50)$$

The cascade theory agrees with the predicted kinetic energy spectrum in winter, as seen in figure 1(c). Between 10-50 km, the simulated spectrum is steeper by about $k^{0.2}$. This anomalous steepening is expected and the difference between the simulated and predicted spectrum is similar to those found in α -turbulence simulations at comparable resolutions (e.g., Pierrehumbert et al. 1994; Schorghofer 2000). However, between 1-5 km, the simulated and predicted slopes nearly coincide. The coincidence of the two

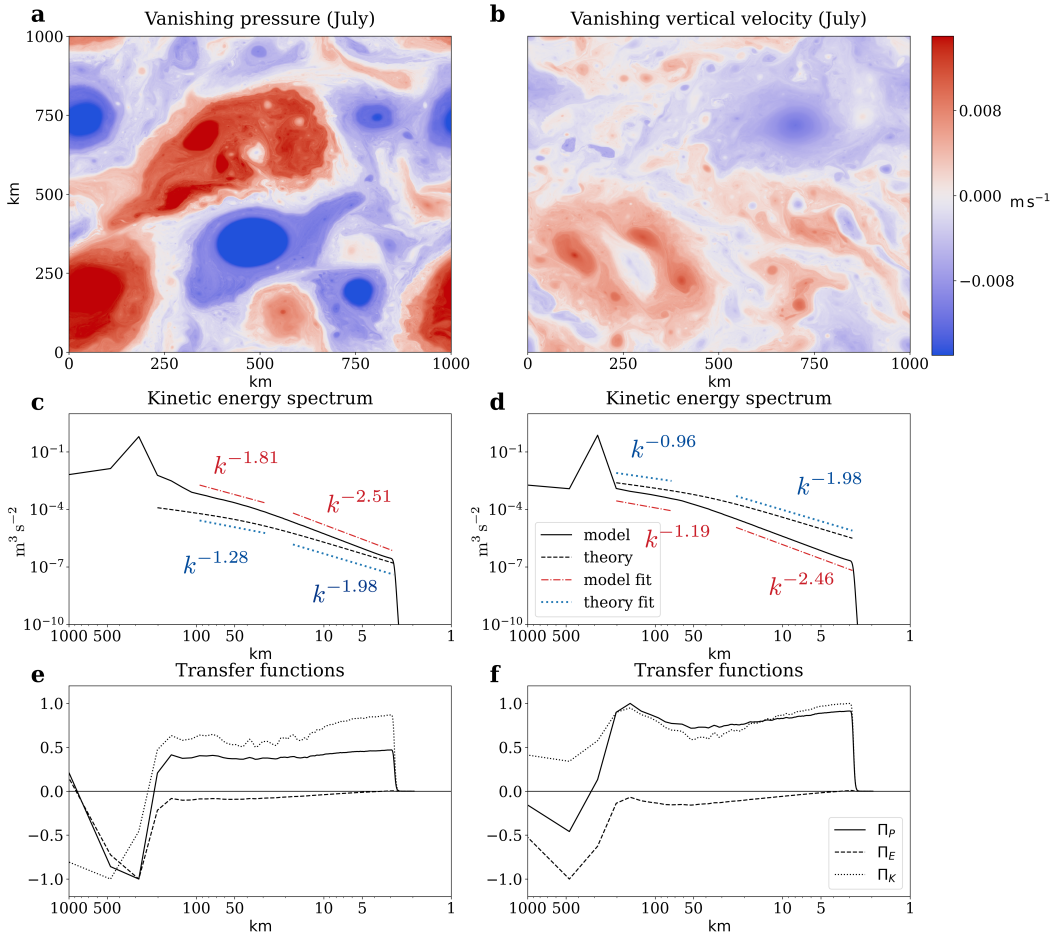


FIG. 6. As in figure 1 but both simulations are in July in a larger, 1000 km \times 1000 km, domain and are forced close to 250 km. The first simulation [panels (a), (c), and (e)] has a Dirichlet bottom boundary condition (48), which corresponds to a vanishing bottom pressure. The second simulation [panels (b), (d), and (f)] has a Neumann bottom boundary condition (49), which corresponds to a vanishing bottom vertical velocity.

spectra is unexpected and may suggest that the theoretical spectrum may be over predicting the steepness of the kinetic energy spectrum.

Whereas the cascade theory succeeds in accounting for the wintertime steepening of the kinetic energy spectrum, figure 1(d) shows that the predicted summertime flattening of the kinetic energy spectrum does not occur. Moreover, even though the predicted kinetic energy spectrum does not have a power law form (except at scales smaller than 10 km), the simulated spectrum develops a clear $\approx k^{-2.3}$ power law between 1-50 km. What determines the slope of this power law is unclear.

An approximate inertial range appears in both wintertime and summertime turbulence [figure 1(d)-(e)]. Therefore, it is not for the lack of an inertial range that the cascade theory fails in summer. Instead, we suggest that the failure is due to the lack of a well-defined power law over a sufficiently wide wavenumber interval. That is, the summertime submesoscales are not scale invariant between 10-100

km [see figure 5(d)]. This lack of scale invariance is due to the stratification's vertical structure. In constant stratification surface quasigeostrophic theory (which is scale invariant), eddies experience the same stratification profile regardless of their horizontal scale. As such, the resulting dynamics do not depend on the horizontal scale of motion. However, for general stratification profiles, smaller eddies experience only the near surface stratification because they decay rapidly in the vertical whereas larger eddies experience more of the stratification's vertical structure because they reach deeper into the ocean. As a consequences, the dynamics depend on the horizontal scale of motion and the predicted spectra are not uniquely determined by dimensional arguments, as discussed in section 3.

The summertime spectrum also depends on the length scale at which forcing is applied, as shown in figure 6. The two simulations in figure 6 differ from those in figure 1 in that they are in a 1000 km \times 1000 km domain and are forced close to 250 km (the simulations in figure 1 have a

400 km \times 400 km domain and are forced close to 100 km). Moreover, both simulations in figure 6 are in July at the same location as the simulations in figure 1. At horizontal scales larger than 400 km, the inversion function depends on the bottom boundary condition. Therefore, in one simulation we use a Dirichlet bottom boundary condition (48), corresponding to vanishing bottom pressure, whereas in the other simulation we use a Neumann bottom boundary condition (49), corresponding to vanishing bottom vertical velocity.

We see in figure 6(c)-(d) that some of the predicted flattening now occurs at horizontal scales larger than 50 km. The degree of flattening differs between the two simulations. The simulated spectrum is steeper than the predicted slope by a factor of $k^{0.5}$ in the vanishing bottom pressure case. In contrast, the simulated spectrum is only $k^{0.25}$ steeper in the vanishing bottom vertical velocity case. Although the simulated spectrum is closest to the predicted spectrum in the case of a vanishing bottom vertical velocity, it is in this case that an inertial range fails to form [see figure 6(f)].

An unexpected consequence of forcing at larger scales is the steepening of the kinetic energy spectrum at scales smaller than 20 km. Instead of a simulated slope of $k^{-2.3}$ observed in figure 1(d), we find the simulated slope is close to $k^{-2.5}$ [figure 6(c)-(d)]. The small-scale steepening of the kinetic energy spectrum occurs whenever the inversion function becomes flatter at larger scales. Indeed, we performed simulations of piecewise α -turbulence, where $m(k) = k^{\alpha_1}$ for $k < k_0$ and $m(k) = C k^{\alpha_2}$ for $k > k_0$ (the constant C is determined by continuity across the two regimes). If forcing is applied at wavenumbers $k < k_0$, we find that if $\alpha_1 < \alpha_2$, the spectrum at $k > k_0$ is significantly steeper than predicted by dimensional arguments (e.g., Pierrehumbert et al. 1994). However, if $\alpha_1 > \alpha_2$, we do not observe such discrepancy.

In the absence of a cascade theory for summertime surface quasigeostrophic turbulence, it is difficult to draw general conclusions for the ocean. The simulations in figures 1 and 6 show that, if we only force at large scales, the kinetic energy spectrum is steeper in winter than in summer. However, oceanic submesoscale turbulence exhibits the opposite seasonality. Perhaps if we account for mixed-layer instability by also forcing at small scales in winter, then we would obtain the correct seasonality. However, this suggestion is beyond the scope of this article.

b. Wintertime kinetic energy spectra and mixed-layer instability

So far, we have been considering the forward cascade kinetic energy spectrum. However, the predicted kinetic energy spectrum generally depends on the horizontal length scale of the forcing. There are two plausible scales at which the submesoscales may be forced.

One possibility is that the submesoscales are mainly forced at small-scales by mixed-layer baroclinic instability (Boccaletti et al. 2007). Several authors have suggested that it is the seasonal cycle in mixed-layer instability that brings about the seasonal cycle in submesoscale turbulence (Sasaki et al. 2014; Qiu et al. 2014; Callies et al. 2016; Uchida et al. 2017). Mixed-layer instability extracts energy from deep wintertime mixed-layers. The resulting turbulence cascades the energy to larger scales and therefore energizes the submesoscales.

If mixed-layer instability is the primary energy source for the submesoscale, then the submesoscales are in the inverse cascade inertial range. We derive the kinetic energy spectrum in this inertial range by using equations (22), (23), and (33) and we find

$$\mathcal{K}(k) \sim \varepsilon_E^{2/3} k^{-1/3} [m(k)]^{-2/3}. \quad (51)$$

Substituting $m(k) \sim k^{3/2}$ into equation (51) gives a $\mathcal{K}(k) \sim k^{-4/3}$ spectrum. This spectrum is much shallower than the observed k^{-2} spectrum. So if the submesoscales are surface quasigeostrophic, then it is unlikely that mixed-layer instability is their primary energy source.

Alternatively, if the submesoscales are forced at large-scales then the submesoscales are in the forward cascade inertial range. Substituting $m(k) \sim k^{3/2}$ into equation (50) gives a $\mathcal{K}(k) \sim k^{-7/3}$ spectrum, which is closer to the observed k^{-2} spectrum. Therefore, if the submesoscales are surface quasigeostrophic, it is more likely that they are mainly forced at large scales.

It is possible that the flattening of the $k^{-7/3}$ kinetic energy spectrum into the observed k^{-2} spectrum is due to mixed-layer instability. If the submesoscales are forced both at large scales and at small scales, then we expect the submesoscale kinetic energy spectrum to be combination of the $k^{-7/3}$ and the $k^{-4/3}$ spectra (Lilly 1989). This dual forcing therefore produces a spectrum flatter than $k^{-7/3}$ with the amount of flattening depending on the ratio of large-scale to small-scale forcing. This suggestion, however, requires further investigation.

c. Vertical structure

Figures 2 and 5 show the vertical structure, $\Psi_k(z)$, to the streamfunction at both 50 km and at 100 km. Comparing each streamfunction with its corresponding stratification profile, we see that the streamfunction is nearly constant in the mixed-layer. It is only below the mixed-layer that the streamfunction begins to decay. The theory is therefore consistent with the vertical structure of submesoscale turbulence (Callies and Ferrari 2013; Sasaki et al. 2014; Callies et al. 2015).

d. Previous work on surface quasigeostrophy with variable stratification

We here comment on earlier studies of surface quasigeostrophy with variable stratification. The first is from LaCasce (2012, 2013) who finds that, in exponential stratification, the surface quasigeostrophic buoyancy variance spectrum is no longer proportional to the kinetic energy spectrum. Indeed, from our equations (22) and (23), we find that the ratio of surface potential enstrophy (which is proportional to buoyancy variance) to kinetic energy is $[m(k)]^2/k^2$. However, LaCasce (2012, 2013) did not pursue the associated implications for surface quasigeostrophic turbulence as considered here.

The second is from Callies and Ferrari (2013) who, in their appendix, consider the predicted kinetic energy spectrum in surface quasigeostrophy with variable stratification. However, they make use of the constant stratification buoyancy variance spectrum of Blumen (1978), namely that $\mathcal{P}(k) \sim k^{-5/3}$. Consequently, their predicted buoyancy variance and kinetic energy spectra (and hence their figure 3) do not fully capture the role of variable stratification. The reason is that, for variable stratification surface quasigeostrophic theory, the buoyancy variance spectrum itself depends on stratification through the inversion function, $m(k)$, as we show in equations (22), (33), and (34).

7. Conclusion

We have described a surface quasigeostrophic theory that takes into account the ocean's variable vertical stratification. The theory shows that the stratification controls the spatial locality of surface quasigeostrophic turbulence. This control provides a physical mechanism relating the kinetic energy spectrum to upper ocean stratification and thus to seasonality. Deep mixed-layers result in a spatially non-local turbulence distinguished by strong small-scale buoyancy gradients and large-scale strain. In contrast, shallow mixed-layers result in a more spatially local turbulence that lacks strong buoyancy gradients and appears diffuse in space.

Over the mid-latitude wintertime open ocean, deep mixed-layers result in a surface quasigeostrophic turbulence whose spatial locality is halfway between two-dimensional vorticity dynamics and constant stratification surface quasigeostrophic dynamics. Moreover, because wintertime surface quasigeostrophic turbulence displays scale invariance across the submesoscales, we can use standard dimensional arguments to determine the cascade spectra.

The summertime surface quasigeostrophic inversion relation is generally not scale invariant at the submesoscales. As such, the cascade theory fails in summer and we lack a general theory for the summertime spectra. If we only force at large scales, our simulations exhibit kinetic energy spectra shallower in summer than in winter. Therefore,

the simulated seasonality is opposite to the seasonality of oceanic submesoscale turbulence.

The dynamics underlying the observed seasonality in submesoscale turbulence therefore remains unclear. However, we remark that the seasonality in upper ocean stratification has two distinct consequences. First, through mixed-layer baroclinic instability, the forcing term F [in the time-evolution equation (5)] is seasonal. Second, the nonlinear dynamics [i.e., the nonlinear Jacobian in the time-evolution equation (5)] are seasonal as well; this second observation constitutes our main contribution.

It is likely that interior quasigeostrophic turbulence exhibits a seasonality analogous to the theory presented here. Charney's theory of interior quasigeostrophic turbulence (Charney 1971) assumes constant stratification and so is unlikely to be valid at the ocean submesoscales. Indeed, the interior quasigeostrophic spectral inversion relation generally depends on both the stratification and the vertical distribution of interior potential vorticity (Smith and Bernard 2013). The seasonality in vertical stratification and interior potential vorticity will then result in a seasonality in interior quasigeostrophic turbulence. However, we leave this suggestion for a future investigation.

Acknowledgments. We thank ... and ... for comments on an early draft. This report was prepared by Houssam Yassin under award NA18OAR4320123 from the National Oceanic and Atmospheric Administration, U.S. Department of Commerce. The statements, findings, conclusions, and recommendations are those of the authors and do not necessarily reflect the views of the National Oceanic and Atmospheric Administration, or the U.S. Department of Commerce.

Data availability statement.

APPENDIX A

The sharp transition limit

We seek a solution to the vertical structure equation (9) for the step-like stratification (39) with upper boundary condition (10) and the infinite lower boundary condition (11). The solution has the form

$$\Psi_k(z) = \cosh(\sigma_0 k z) + a_2 \sinh(\sigma_0 k z) \quad (\text{A1})$$

for $-h_{\text{mix}} \leq z \leq 0$, and

$$\Psi_k(z) = a_3 e^{\sigma_{\text{pyc}} k(z+h_{\text{mix}})} \quad (\text{A2})$$

for $-\infty < z < -h_{\text{mix}}$. To determine a_2 and a_3 , we require $\Psi_k(z)$ to be continuous across $z = -h_{\text{mix}}$ and that its derivative satisfy

$$\frac{1}{\sigma_0^2} \frac{d\Psi_k(-h_{\text{mix}}^+)}{dz} = \frac{1}{\sigma_{\text{pyc}}^2} \frac{d\Psi_k(-h_{\text{mix}}^-)}{dz} \quad (\text{A3})$$

where the $-$ and $+$ superscripts indicate limits from the below and above respectively. Solving for a_2 and substituting equation (A1) into equation (15) then yields the inversion function $m(k)$.

APPENDIX B

The numerical model

We solve equation (5) using the pseudo-spectral `pyqg` model (Abernathy et al. 2019). To take stratification into account, we use the inversion relation (14). Given a stratification profile $\sigma(z)$ from ECCOV4, we first interpolate the ECCOV4 stratification profile with a cubic spline onto a vertical grid with 350 vertical grid points. We then numerically solve equation (9), along with boundary conditions (10) and either (48) or (49), and obtain the vertical structure at each wavevector k . Using equation (15) then gives the inversion function $m(k)$.

We apply a large-scale forcing, F , between the (non-dimensional) wavenumbers $3.5 < k < 4.5$ in all our simulations, corresponding to horizontal length scales 88 - 114 km in the figure 1 simulations and 222-286 km in the figure 6 simulations. Otherwise, the forcing F is as in Smith et al. (2002). The dissipation term can be written as

$$D = r_d \theta + \text{ssd} \quad (\text{B1})$$

where r_d is a damping rate and `ssd` is small-scale dissipation. Small-scale dissipation is through an exponential potential enstrophy filter as in Arbic and Flierl (2003). Simulations have a horizontal resolution of 1024^2 horizontal grid points.

References

- Abernathy, R., and Coauthors, 2019: `pyqg/pyqg`: v0.3.0. Zenodo, <https://doi.org/10.5281/zenodo.3551326>.
- Arbic, B. K., and G. R. Flierl, 2003: Coherent vortices and kinetic energy ribbons in asymptotic, quasi two-dimensional f-plane turbulence. *Physics of Fluids*, **15**, 2177–2189, <https://doi.org/10.1063/1.1582183>.
- Blumen, W., 1978: Uniform Potential Vorticity Flow: Part I. Theory of Wave Interactions and Two-Dimensional Turbulence. *J. Atmos. Sci.*, **35**, 774–783, [https://doi.org/10.1175/1520-0469\(1978\)035<0774:UPVFPI>2.0.CO;2](https://doi.org/10.1175/1520-0469(1978)035<0774:UPVFPI>2.0.CO;2).
- Boccaletti, G., R. Ferrari, and B. Fox-Kemper, 2007: Mixed Layer Instabilities and Restrification. *J. Phys. Oceanogr.*, **37**, 2228–2250, <https://doi.org/10.1175/JPO3101.1>.
- Bretherton, F. P., 1966: Critical layer instability in baroclinic flows. *Quart. J. Roy. Meteor. Soc.*, **92**, 325–334, <https://doi.org/10.1002/qj.49709239302>.
- Callies, J., and R. Ferrari, 2013: Interpreting Energy and Tracer Spectra of Upper-Ocean Turbulence in the Submesoscale Range (1–200 km). *J. Phys. Oceanogr.*, **43**, 2456–2474, <https://doi.org/10.1175/JPO-D-13-063.1>.
- Callies, J., R. Ferrari, J. M. Klymak, and J. Gula, 2015: Seasonality in submesoscale turbulence. *Nature*, **6**, <https://doi.org/10.1038/ncomms7862>.
- Callies, J., G. Flierl, R. Ferrari, and B. Fox-Kemper, 2016: The role of mixed-layer instabilities in submesoscale turbulence. *J. Fluid Mech.*, **788**, 5–41, <https://doi.org/10.1017/jfm.2015.700>, <https://doi.org/10.1017/jfm.2015.700>.
- Charney, J. G., 1971: Geostrophic Turbulence. *J. Atmos. Sci.*, **28**, 1087–1095, [https://doi.org/10.1175/1520-0469\(1971\)028<1087:GT>2.0.CO;2](https://doi.org/10.1175/1520-0469(1971)028<1087:GT>2.0.CO;2).
- Forget, G., J.-M. Campin, P. Heimbach, C. N. Hill, R. M. Ponte, and C. Wunsch, 2015: ECCO version 4: an integrated framework for non-linear inverse modeling and global ocean state estimation. *Geoscientific Model Development*, **8**, 3071–3104, <https://doi.org/10.5194/gmd-8-3071-2015>.
- Gkioulekas, E., and K. K. Tung, 2007: A new proof on net upscale energy cascade in two-dimensional and quasi-geostrophic turbulence. *J. Fluid Mech.*, **576**, 173–189, <https://doi.org/10.1017/S0022112006003934>.
- Held, I. M., R. T. Pierrehumbert, S. T. Garner, and K. L. Swanson, 1995: Surface quasi-geostrophic dynamics. *J. Fluid Mech.*, **282**, 1–20, <https://doi.org/10.1017/S0022112095000012>.
- Kraichnan, R. H., 1967: Inertial Ranges in Two-Dimensional Turbulence. *Physics of Fluids*, **10**, 1417–1423, <https://doi.org/10.1063/1.1762301>.
- LaCasce, J. H., 2012: Surface Quasigeostrophic Solutions and Baroclinic Modes with Exponential Stratification. *J. Phys. Oceanogr.*, **42**, 569–580, <https://doi.org/10.1175/JPO-D-11-0111.1>.
- LaCasce, J. H., 2013: Corrigendum to Surface Quasigeostrophic Solutions and Baroclinic Modes with Exponential Stratification. *J. Phys. Oceanogr.*, **43**, 1838–1839, <https://doi.org/10.1175/JPO-D-13-050.1>.
- LaCasce, J. H., and A. Mahadevan, 2006: Estimating subsurface horizontal and vertical velocities from sea-surface temperature. *J. Mar. Res.*, **64**, 695–721, <https://doi.org/10.1357/002224006779367267>.
- Lapeyre, G., and P. Klein, 2006: Dynamics of the Upper Oceanic Layers in Terms of Surface Quasigeostrophy Theory. *J. Phys. Oceanogr.*, **36**, 165–176, <https://doi.org/10.1175/JPO2840.1>.
- Larichev, V. D., and J. C. McWilliams, 1991: Weakly decaying turbulence in an equivalent-barotropic fluid. *Physics of Fluids A: Fluid Dynamics*, **3**, 938–950, <https://doi.org/10.1063/1.857970>.
- Lilly, D. K., 1989: Two-Dimensional Turbulence Generated by Energy Sources at Two Scales. *J. Atmos. Sci.*, **46**, 2026–2030, [https://doi.org/10.1175/1520-0469\(1989\)046<2026:TDTGBE>2.0.CO;2](https://doi.org/10.1175/1520-0469(1989)046<2026:TDTGBE>2.0.CO;2).
- Mensa, J. A., Z. Garraffo, A. Griffa, T. M. Özgökmen, A. Haza, and M. Veneziani, 2013: Seasonality of the submesoscale dynamics in the Gulf Stream region. *Ocean Dynamics*, **63**, 923–941, <https://doi.org/10.1007/s10236-013-0633-1>.
- Pierrehumbert, R. T., I. M. Held, and K. L. Swanson, 1994: Spectra of local and nonlocal two-dimensional turbulence. *Chaos, Solitons & Fractals*, **4**, 1111–1116, [https://doi.org/10.1016/0960-0779\(94\)90140-6](https://doi.org/10.1016/0960-0779(94)90140-6).
- Polvani, L. M., N. J. Zabusky, and G. R. Flierl, 1989: Two-layer geostrophic vortex dynamics. Part 1. Upper-layer V-states

- and merger. *J. Fluid Mech.*, **205**, 215–242, <https://doi.org/10.1017/S0022112089002016>.
- Qiu, B., S. Chen, P. Klein, H. Sasaki, and Y. Sasai, 2014: Seasonal Mesoscale and Submesoscale Eddy Variability along the North Pacific Subtropical Countercurrent. *J. Phys. Oceanogr.*, **44**, 3079–3098, <https://doi.org/10.1175/JPO-D-14-0071.1>.
- Rocha, C. B., T. K. Chereskin, S. T. Gille, and D. Menemenlis, 2016: Mesoscale to Submesoscale Wavenumber Spectra in Drake Passage. *J. Phys. Oceanogr.*, **46**, 601–620, <https://doi.org/10.1175/JPO-D-15-0087.1>.
- Sasaki, H., P. Klein, B. Qiu, and Y. Sasai, 2014: Impact of oceanic-scale interactions on the seasonal modulation of ocean dynamics by the atmosphere. *Nature Communications*, **5**, <https://doi.org/10.1038/ncomms6636>.
- Schorghofer, N., 2000: Energy spectra of steady two-dimensional turbulent flows. *Physical Review E*, **61**, 6572–6577, <https://doi.org/10.1103/PhysRevE.61.6572>.
- Shcherbina, A. Y., E. A. D’Asaro, C. M. Lee, J. M. Klymak, M. J. Molemaker, and J. C. McWilliams, 2013: Statistics of vertical vorticity, divergence, and strain in a developed submesoscale turbulence field. *Geophys. Res. Lett.*, **40**, 4706–4711, <https://doi.org/10.1002/grl.50919>.
- Smith, K. S., and E. Bernard, 2013: Geostrophic turbulence near rapid changes in stratification. *Physics of Fluids*, **25**, <https://doi.org/10.1063/1.4799470>.
- Smith, K. S., G. Boccaletti, C. C. Henning, I. Marinov, C. Y. Tam, I. M. Held, and G. K. Vallis, 2002: Turbulent diffusion in the geostrophic inverse cascade. *J. Fluid Mech.*, **469**, 13–48, <https://doi.org/10.1017/S0022112002001763>.
- Su, Z., J. Wang, P. Klein, A. F. Thompson, and D. Menemenlis, 2018: Ocean submesoscales as a key component of the global heat budget. *Nature Communications*, **9**, <https://doi.org/10.1038/s41467-018-02983-w>.
- Thompson, A. F., A. Lazar, C. Buckingham, A. C. N. Garabato, G. M. Damerell, and K. J. Heywood, 2016: Open-Ocean Submesoscale Motions: A Full Seasonal Cycle of Mixed Layer Instabilities from Gliders. *J. Phys. Oceanogr.*, **46**, 1285–1307, <https://doi.org/10.1175/JPO-D-15-0170.1>.
- Tulloch, R., and K. S. Smith, 2006: A theory for the atmospheric energy spectrum: Depth-limited temperature anomalies at the tropopause. *Proc. Natl. Acad. Sci. (USA)*, **103**, 14 690–14 694, <https://doi.org/10.1073/pnas.0605494103>.
- Uchida, T., R. Abernathey, and S. Smith, 2017: Seasonality of eddy kinetic energy in an eddy permitting global climate model. *Ocean Modelling*, **118**, 41–58, <https://doi.org/10.1016/j.ocemod.2017.08.006>.
- Wang, D.-P., C. N. Flagg, K. Donohue, and H. T. Rossby, 2010: Wavenumber Spectrum in the Gulf Stream from Shipboard ADCP Observations and Comparison with Altimetry Measurements. *J. Phys. Oceanogr.*, **40**, 840–844, <https://doi.org/10.1175/2009JPO4330.1>.